AIP | Applied Physics Letters

Quasi-particle electronic band structure and alignment of the V-VI-VII semiconductors SbSI, SbSBr, and SbSeI for solar cells

Keith T. Butler, Scott McKechnie, Pooya Azarhoosh, Mark van Schilfgaarde, David O. Scanlon, and Aron Walsh

Citation: Applied Physics Letters **108**, 112103 (2016); doi: 10.1063/1.4943973
View online: http://dx.doi.org/10.1063/1.4943973
View Table of Contents: http://scitation.aip.org/content/aip/journal/apl/108/11?ver=pdfcov
Published by the AIP Publishing

Quasi-particle electronic band structure and alignment of the V-VI-VII semiconductors SbSI, SbSBr, and SbSeI for solar cells

Keith T. Butler,[1] Scott McKechnie,[2] Pooya Azarhoosh,[2] Mark van Schilfgaarde,[2] David O. Scanlon,[3,4] and Aron Walsh[1,5,a)]
[1]*Centre for Sustainable Chemical Technologies and Department of Chemistry, University of Bath, Claverton Down, Bath BA2 7AY, United Kingdom*
[2]*Department of Physics, Kings College London, London WC2R 2LS, United Kingdom*
[3]*University College London, Kathleen Lonsdale Materials Chemistry, 20 Gordon Street, London WC1H 0AJ, United Kingdom*
[4]*Diamond Light Source Ltd., Diamond House, Harwell Science and Innovation Campus, Didcot, Oxfordshire OX11 0DE, United Kingdom*
[5]*Global E[3] Institute and Department of Materials Science and Engineering, Yonsei University, Seoul 120-749, South Korea*

(Received 25 November 2015; accepted 2 March 2016; published online 15 March 2016)

The ternary V-VI-VII chalcohalides consist of one cation and two anions. Trivalent antimony—with a distinctive $5s^2$ electronic configuration—can be combined with a chalcogen (e.g., S or Se) and halide (e.g., Br or I) to produce photoactive ferroelectric semiconductors with similarities to the Pb halide perovskites. We report—from relativistic quasi-particle self-consistent *GW* theory—that these materials have a multi-valley electronic structure with several electron and hole basins close to the band extrema. We predict ionisation potentials of 5.3–5.8 eV from first-principles for the three materials, and assess electrical contacts that will be suitable for achieving photovoltaic action from these unconventional compounds. © *2016 AIP Publishing LLC*.
[http://dx.doi.org/10.1063/1.4943973]

Building on the success of elemental semiconductors, binary II-VI (e.g., CdTe) and III-V (e.g., GaAs) semiconductors have been widely studied for application in solar energy conversion. More recently, the chalcopyrite I_2-III-VI_2, perovskite I-II-VII_3, and kesterite I_2-II-IV-VI_4 systems have gathered significant interest and increasingly high light-to-electricity conversion efficiency in photovoltaic devices.[1]

A common feature of these multi-component semiconductors is that they combine multiple cations (or metals) with a single anion. One potential issue arises where species with similar size and co-ordination preferences are present in the same material, which can lead to the formation of anti-site defects in high concentrations. Cation disorder has been observed in systems ranging from $ZnSnP_2$[2,3] to Cu_2ZnSnS_4[4,5] and is typically associated with poor photovoltaic performance (low open-circuit voltages resulting from high electron-hole recombination rates).[6,7]

V-VI-VII semiconductors are interesting chemically as they are ternary materials, usually formed of a trivalent cation with divalent and monovalent anions. From this family of compounds, SbSI (see Fig. 1) was extensively studied in the 1960s as a photoactive ferroelectric semiconductor.[8–12] The Curie temperature for phase transition between the polar ($Pna2_1$, C_{2v} symmetry) and paraelectric phases (Pnam, D_{2h} symmetry) was measured to be 295 K.[8] In this structure class, *c* is the polar axis and the phase transition is associated with a shift in the Sb and S sublattice with respect to I along this direction.[13]

The ferroelectric behaviour of SbSI can be associated with the $5s^2$ lone pair electrons of Sb^{3+}. As with other group 14 and 15 cations (e.g., Pb^{2+}, Sn^{2+}, Bi^{3+}), a second-order Jahn-Teller instability can exist, which is associated with the change from a symmetric to asymmetric coordination environment of the cation with on-site *s–p* hybridisation.[15,16] SbSI exhibits an optical band gap of ∼2 eV, and the value can be tuned by the choice of chalcogen and halide.[17] The reference optical band gaps of SbSI, SbSBr, and SbSeI fall in the range 1.7–2.2 eV.[18] The predicted electron and hole effective masses are less than 1 m_e,[19] while the static dielectric constant is ∼70,[20] consistent with its tendency for spontaneous polarisation.

The application of ferroelectric materials for solar energy conversion has enjoyed a recent renaissance. The coexistence of photo-activated electron hole generation and an intrinsic electric field offers the opportunity for simultaneous charge carrier generation and separation in the bulk material. There has been success in the application of ferroelectric perovskite oxides,[21] and suggestions that the polarisation of hybrid perovskites contributes to their high-performance.[22–24] We discussed the physics underpinning photoactive ferroelectrics in a recent perspective review, which also looked at the V-VI-VII semiconductors as an interesting case study.[19] The materials also emerged in a subsequent theoretical screening of defect tolerant semiconductors.[20]

Sb-based V-VI-VII materials combine near visible-range absorption with polar instabilities and represent a promising class of photovoltaic absorbers. In this letter, we consider the band structure, ionisation potentials (IPs), and electron affinities (EAs) of several promising V-VI-VII compounds, in order to facilitate device design, in particular, suggesting optimal contact layers to achieve efficient charge extraction.

a)Electronic mail: a.walsh@bath.ac.uk

The crystal structures of SbSI, SbSBr, and SbSeI were fully optimised, using the set-up previously described,[19] with density functional theory (DFT) under periodic boundary conditions. In this study, only the room temperature non-polar phase is considered. Reciprocal space sampling of $3 \times 2 \times 6$ *k*-points was used for the bulk calculations, with a single *k*-point normal to the surface termination for the vacuum level (VL) calculations. Electronic structure information was obtained with the local density approximation (LDA) and using a screened hybrid functional (HSE06).[25,26] Parallelism across *k*-points was performed to utilise up to 512 computing cores.[27] In order to provide quantitative electronic structure information, additional calculations were performed using self-consistent quasi-particle *GW* theory[28] (QS*GW*) as implemented in the all-electron (linear muffin tin orbital basis) package LMSuite.[29] Starting from calculations within the LDA, self-consistency of the quasi-particle states was performed for each material including spin-orbit coupling within the formalism recently reported for the hybrid perovskite $CH_3NH_3PbI_3$.[30]

To calculate the IP, the non-polar (**110**) termination was cut from the relaxed bulk structure using a slab thickness of 4 layers (~30 Å) and vacuum thickness of 30 Å. Alignment of the VL to the valence band maximum (VBM) was performed using the package MacroDensity.[31] The electron removal energy is calculated from LDA-DFT, but includes spin-orbit coupling effects (Δ_{SOC}) and a quasi-particle correction from the bulk material ($\Delta\epsilon_{QSGW}$) according to

$$\Phi_{IP} = \epsilon_{DFT}^{VBM} + \Delta_{SOC} + \Delta\epsilon_{QSGW}^{VBM} - VL. \quad (1)$$

The corresponding EA is found by subtracting the value of the QS*GW* band gap, i.e., EA = IP - E_g. The various contributions to the IP are reported in the supplementary material.[32]

A representative electronic band structure of SbSBr is shown in Figure 2. Here, the quasi-particle corrections increase the magnitude of the band gap, but do not alter the dispersion in reciprocal space. This is in contrast to $CH_3NH_3PbI_3$, where large many-body renormalisation occurs,[30] and has the benefit that a simple "scissors" correction to a DFT band structure can provide a reasonable description of the valence and conduction bands. The associated band parameters for all materials are summarised in Table I.

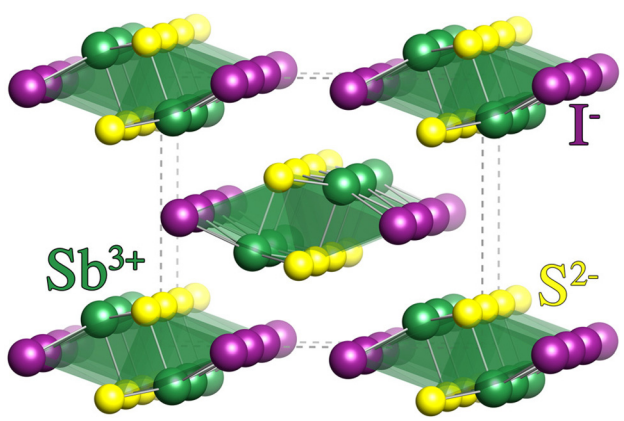

FIG. 1. Representation of the crystal structure of SbSI (Pnam phase) consisting of pseudo-1D channels. These channels are bridged by a long Sb–I bond (3.87 Å), which compares to intra-chain separations of 2.5 and 2.7 Å. Analysis of the electronic structure confirms that this structural motif is due to a stereochemically active lone pair, a feature of other Sb compounds.[14]

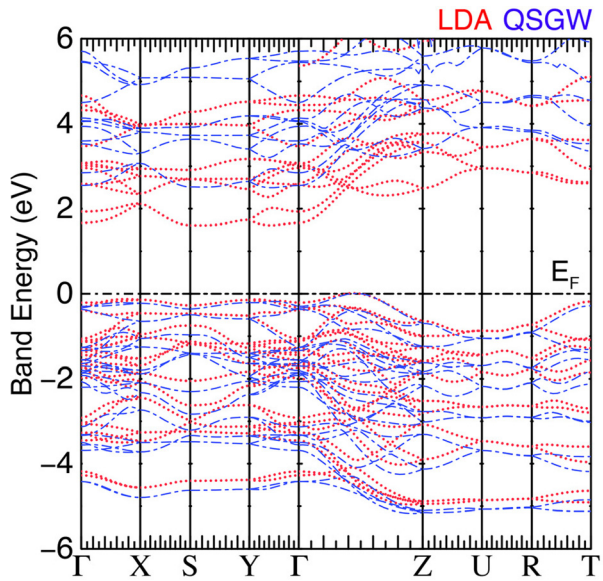

FIG. 2. Electronic band structure of SbSBr from LDA (dotted lines) and quasi-particle self-consistent *GW* theory (dashed lines) including spin-orbit coupling. The highest occupied state (E_F) is set to 0 eV. Note that the band gap is indirect, with the valence band maximum lying along $\Gamma \rightarrow Z$ and the conduction band minimum lying along $\Gamma \rightarrow Y$.

SbSI, SbSBr, and SbSeI have indirect band gaps, each with a conduction band minimum (CBM) in the *xy* plane (bounded by the triangle between the Γ, Y and S special *k*-points). The mirror and inversion operations yield four symmetry equivalent points. In each case, the next nearest minimum is multiples of k_BT (T = 300 K) higher in energy. SbSI has a valence band maximum between U and X, that is two-fold symmetry degenerate, and a second maximum (within k_BT of the global maximum) between Γ and Z that is also two-fold degenerate. Substitution of I by Br in SbSBr results in a VBM (with two-fold degeneracy) between Γ and Z that is multiples of k_BT higher than the next maximum. Substitution of S by Se in SbSeI also produces a lone VBM (two-fold degenerate), close to the Y point, on the line between Γ and Y. The difference between direct and indirect band gaps is around 0.2 eV. The consequences of this unusual band dispersion are that optical absorption (vertical transitions) will be strong due to the high degeneracy of bands, while electron-hole recombination should be suppressed due to thermalisation of carriers to basins of different electron momentum.

TABLE I. Calculated electronic band gap (E_g), ionisation potential (IP), and electron affinity (EA) of three V-VI-VII semiconductors. Results are shown for both density functional theory (HSE06 hybrid functional) and many-body QS*GW* theory. All values include spin-orbit coupling (the contribution is given by Δ_{SOC}) and are in eV. Note that the band gaps exclude finite-temperature and excitonic effects. Effective masses for the valence (m_h^*) and conduction (m_e^*) bands are given in units of m_e.

Material	E_g^{HSE06}	E_g^{QSGW}	m_e^*	m_h^*	Δ_{SOC}	IP	EA
SbSI	2.11	2.22	0.43	0.57	−0.16	5.37	3.15
SbSBr	2.31	2.53	0.51	0.64	−0.11	5.80	3.37
SbSeI	1.86	2.03	0.54	0.58	−0.18	5.26	3.23

Therefore, these systems in principle combine the benefits of direct and indirect band gap materials.

The isotropic electron and hole effective masses are all calculated to be below 0.65 m_e, which can support high-mobility band transport. The values shown in Table I are obtained via a geometric mean of the eigenvalues along the principal axes of an ellipsoidal fit. The effective masses are found to be larger for higher lying extrema, e.g., the second valence band maximum of SbSI has an isotropic effective mass of 0.92 m_e.

The calculated band gaps in Table I show that the QS*GW* value is slightly larger than for HSE06. The energies compare well to available experimental data (2.07 eV (Ref. 33) and 2.11 eV (Ref. 17) for SbSI, 1.76 eV (Ref. 34) and 1.67 eV (Ref. 17) for SbSeI, and 2.18 eV (Ref. 17) for SbSBr) but are consistently overestimated. There are two main sources of error here: first, they omit renormalisation of the gap from the electron-phonon interaction. Second, the ladder diagrams coupling electrons and holes are omitted. These two effects together largely account for the well known overestimation of QS*GW* gaps. In contrast to other approaches such as hybrid DFT, the theory is true *ab initio* (parameter-free). Moreover, the errors are systematic for a wide range of materials, including most semiconductors.[28] There may be a further discrepancy because of uncertainties in structure, and also in the experimental values themselves. SbSI, for example, has a strong negative band gap deformation potential with increased temperature.[33]

The predicted ionisation potentials for SbSI, SbSBr, and SbSeI are 5.37, 5.80, and 5.26 eV, respectively (Table I). These values are referenced to a bulk calculation and are therefore exclusive of surface state contributions. We found a relatively small contribution of <0.25 eV from surface states in all cases. There are no strong interatomic bonds broken to form the surface, which contrasts to structures where states are produced by bond breaking (e.g., dangling bonds); for example, a surface contribution of 1.16 eV was found in SnO_2.[36] The IP values exclude the effects of interfacial strain and chemical interactions that may influence the band offset at a particular interface; however, they offer a good first approximation of the band alignment of a single phase material, as evidenced by the widespread application of Anderson's rule[37] for estimating band offsets.

The predicted band energies are compared to other common materials for solar energy conversion in Figure 3. The positions of the band edges are related closely to the nature of the halide ion; the band edge states are largely composed of the halide electronic states. The valence band of SbSBr is therefore significantly deeper in energy than the iodide materials. SbSBr is similar in energy to several Cu based photoabsorbers—these include Cu_2ZnSnS_4 (CZTS), Cu_2S, and $CuInS_2$—where the upper valence band is composed of Cu 3d states;[38] therefore, similar contacting materials to the copper materials could be applied for SbSBr. The difference in the energy levels for the iodide-containing compounds means that alternative contact materials are necessary for optimal performance. This point was recently demonstrated for layered Sn-based photoabsorbers, which exhibit even lower ionisation potentials.[39,40] Although both Sb(III) and Sn(II) feature a $5s^25p^0$ electronic configuration, the lower nuclear charge and oxidation state of Sn decreases their binding energy and hence ionisation potential of the Sn(II) materials.

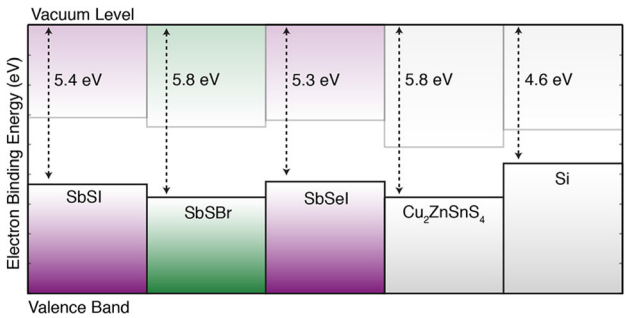

FIG. 3. Calculated ionisation levels of SbSI, SbSBr, and SbSeI, with respect to the vacuum level. Also shown for comparison are values for Si and Cu_2ZnSnS_4 adapted from Ref. 35.

A common architecture for thin-film solar cells—inherited from $CuInSe_2$ technology and used in CZTS solar cells—is a back-contact of Mo-coated glass, which is responsible for hole collection. Electron collection is facilitated by a buffer layer of CdS towards a transparent conducting oxide such as ZnO or $CdSnO_3$. All three V-VI-VII semiconductors have relatively low electron affinities, so an alternative electron contact would be required. CdS can be replaced by a tunable (Cd,Zn)S or Zn(O,S) alloy. Applying the electronic matching criteria from a recently reported method for screening semiconductor contacts,[41] we suggest can further suggest ZnTe, Cu_2O, Zn_2TiO_4, $KTaO_3$, $AlTiO_3$, and $MgTiO_3$ as potential replacements for CdS. For the hole-collecting contact, since SbSBr has a similar valence band energy to CZTS, Mo should still suffice. SbSI and SbSeI have lower binding energy valence bands and possible candidates for replacing Mo include Au or Ni, which have well matched workfunctions. Due to the wide band gaps of these V-VI-VII semiconductors, they could also find potential application in low-cost tandem solar cells or in solar fuel applications where higher voltages (over-potentials) are required.

In summary, we have analysed the electronic structure of three V-VI-VII semiconductors. Owing to the unusual crystal structures, the electronic band dispersion is complex with multiple valleys close to the valence and conduction band extrema, which is expected to result in non-conventional photo-physical behaviour. These Sb-based compounds display expected chemical trends with smaller band gaps found for heavier chalcogenide and halide compositions. These trends also appear to be observed in the Bi-based compounds.[42] We predict their ionisation potentials compared to common active layers in thin-film solar cells, and suggest that alternative contact materials should be considered in order to optimise performance. The smallest band gap of 2 eV is calculated for SbSeI, which is at the upper end for application in single-junction solar cells. The replacement of Se by Te to form SbTeBr and SbTeI may provide a route to further red-shift the optical response, albeit at the cost of elemental abundance and sustainability.

We thank J. M. Frost for useful discussions, and acknowledge membership of the UK's HPC Materials

Chemistry Consortium, which is funded by EPSRC Grant No. EP/L000202. The work has also been supported by EPSRC through Grant Nos. EP/M009580/1, EP/J017361/1, EP/M009602/1, and EP/M011631/1. This work benefited from membership of the UK Materials Design Network. *Data access statement:* The crystal structures reported in this work are available in an on-line repository https://github.com/WMD-group/Crystal_ structures and the MacroDensity code is freely available from https://github.com/WMD-group/MacroDensity.

[1]M. A. Green, A. Ho-Baillie, and H. J. Snaith, Nat. Photonics **8**, 506 (2014).
[2]D. O. Scanlon and A. Walsh, Appl. Phys. Lett. **100**, 251911 (2012).
[3]T. Yokoyama, F. Oba, A. Seko, H. Hayashi, Y. Nose, and I. Tanaka, Appl. Phys. Express **6**, 061201 (2013).
[4]J. J. S. Scragg, L. Choubrac, A. Lafond, T. Ericson, and C. Platzer-Björkman, Appl. Phys. Lett. **104**, 041911 (2014).
[5]S. Chen, A. Walsh, X.-G. Gong, and S.-H. Wei, Adv. Mater. **25**, 1522 (2013).
[6]T. Gokmen, O. Gunawan, T. K. Todorov, and D. B. Mitzi, Appl. Phys. Lett. **103**, 103506 (2013).
[7]O. Gunawan, T. Gokmen, and D. B. Mitzi, J. Appl. Phys. **116**, 084504 (2014).
[8]E. Fatuzzo, G. Harbeke, W. J. W. Merz, R. Nitsche, H. Roetschi, and W. Ruppel, Phys. Rev. **127**, 2036 (1962).
[9]R. Nitsche, H. Roetschi, and P. Wild, Appl. Phys. Lett. **4**, 210 (1964).
[10]D. Berlincourt, H. Jaffe, W. J. Merz, and R. Nitsche, Appl. Phys. Lett. **4**, 61 (1964).
[11]V. M. Fridkin, I. I. Groshik, V. A. Lakhovizkaya, M. P. Mikhailov, and V. N. Nosov, Appl. Phys. Lett. **10**, 354 (1967).
[12]A. A. Grekov, A. I. Rodin, and V. M. Fridkin, Appl. Phys. Lett. **14**, 119 (1969).
[13]A. Kikuchi, Y. Oka, and E. Sawaguchi, J. Phys. Soc. Jpn. **23**, 337 (1967).
[14]J. P. Allen, J. J. Carey, A. Walsh, D. O. Scanlon, and G. W. Watson, J. Phys. Chem. C **117**, 14759 (2013).
[15]D. J. Payne, R. G. Egdell, A. Walsh, G. W. Watson, J. Guo, P.-A. Glans, T. Learmonth, and K. E. Smith, Phys. Rev. Lett. **96**, 157403 (2006).
[16]A. Walsh, D. J. Payne, R. G. Egdell, and G. W. Watson, Chem. Soc. Rev. **40**, 4455 (2011).
[17]J. Alward and C. Fong, Solid State Commun. **25**, 307 (1978).
[18]O. M. Madelung, *Semiconductors: Data Handbook*, 3rd ed. (Springer, Berlin, 2003), p. 691.
[19]K. T. Butler, J. M. Frost, and A. Walsh, Energy Environ. Sci. **8**, 838 (2015).
[20]R. E. Brandt, V. Stevanović, D. S. Ginley, and T. Buonassisi, MRS Commun. **5**, 265 (2015).
[21]R. Nechache, C. Harnagea, S. Li, L. Cardenas, W. Huang, J. Chakrabartty, and F. Rosei, Nat. Photonics **9**, 61 (2015).
[22]J. M. Frost, K. T. Butler, F. Brivio, C. H. Hendon, M. van Schilfgaarde, and A. Walsh, Nano Lett. **14**, 2584 (2014).
[23]Y. Kutes, L. Ye, Y. Zhou, S. Pang, B. D. Huey, and N. P. Padture, J. Phys. Chem. Lett. **5**, 3335 (2014).
[24]S. N. Rashkeev, F. El-Mellouhi, S. Kais, and F. H. Alharbi, Sci. Rep. **5**, 11467 (2015).
[25]J. Heyd and G. Scuseria, J. Chem. Phys. **121**, 1187 (2004).
[26]J. Heyd, G. E. Scuseria, and M. Ernzerhof, J. Chem. Phys. **124**, 219906 (2006).
[27]A. Maniopoulou, E. R. Davidson, R. Grau-Crespo, A. Walsh, I. J. Bush, C. R. A. Catlow, and S. M. Woodley, Comput. Phys. Commun. **183**, 1696 (2012).
[28]M. Van Schilfgaarde, T. Kotani, and S. Faleev, Phys. Rev. Lett. **96**, 226402 (2006).
[29]See http://www.lmsuite.org for Lmsuite; accessed 12 December 2015.
[30]F. Brivio, K. T. Butler, A. Walsh, and M. van Schilfgaarde, Phys. Rev. B **89**, 155204 (2014).
[31]K. T. Butler, C. H. Hendon, and A. Walsh, Appl. Mater. Interfaces **6**, 22044 (2014).
[32]See supplementary material at http://dx.doi.org/10.1063/1.4943973 for additional calculation details.
[33]M. Nowak and P. Szperlich, Opt. Mater. **35**, 1200 (2013).
[34]T. A. Pikka and V. M. Fridkin, Fiz. Tverd. Tela **10**, 2668 (1969).
[35]K. T. Butler, J. M. Frost, and A. Walsh, Mater. Horiz. **2**, 228 (2015).
[36]K. T. Butler, J. Buckeridge, C. R. A. Catlow, and A. Walsh, Phys. Rev. B **89**, 115320 (2014).
[37]R. Anderson, Solid State Electron. **5**, 341 (1962).
[38]S. H. Wei and A. Zunger, J. Appl. Phys. **78**, 3846 (1995).
[39]L. A. Burton and A. Walsh, Appl. Phys. Lett. **102**, 132111 (2013).
[40]V. Steinmann, R. Jaramillo, K. Hartman, R. Chakraborty, R. E. Brandt, J. R. Poindexter, Y. S. Lee, L. Sun, A. Polizzotti, H. H. Park, R. G. Gordon, and T. Buonassisi, Adv. Mater. **26**, 7488 (2014).
[41]K. T. Butler, Y. Kumagai, F. Oba, and A. Walsh, J. Mater. Chem. C **4**, 1149 (2016).
[42]A. M. Ganose, K. T. Butler, A. Walsh, and D. O. Scanlon, J. Mater. Chem. A **4**, 2060 (2016).